Materials Research Express

PAPER • **OPEN ACCESS**

Conversion of water and carbon dioxide into methanol with solar energy on Au/Co nanostructured surfaces

To cite this article: Qinghua Zhu *et al* 2020 *Mater. Res. Express* **7** 035014

Materials Research Express

OPEN ACCESS

RECEIVED
30 November 2019

REVISED
28 February 2020

ACCEPTED FOR PUBLICATION
5 March 2020

PUBLISHED
16 March 2020

PAPER

Conversion of water and carbon dioxide into methanol with solar energy on Au/Co nanostructured surfaces

Qinghua Zhu, Cong Wang, Haizhou Ren, Ming Zeng, Zhe Kan , Zibo Wang and Mengyan Shen

Department of Physics and Applied Physics, and Nanomanufacturing Center, University of Massachusetts Lowell, 1 University Avenue, Lowell, Massachusetts 01854, United States of America

E-mail: mengyan_shen@uml.edu

Keywords: nanoparticle, artificial photosynthesis, carbon dioxide, methanol

Supplementary material for this article is available online

Abstract

Conversion of carbon dioxide (CO_2) and water (H_2O) to methanol (CH_3OH) is achieved through an artificial photosynthesis procedure utilizing cobalt (Co) micro-particle based photocatalyst and solar energy in a simple, closed reactor. The photocatalyst is fabricated by exposing the surfaces of cobalt microparticles to femtosecond laser irradiation in a gold chloride (AuCl) solution. The morphology and composite of the photocatalyst surfaces were observed and detected to be a layer of cobalt dioxide (CoO) nano-flakes on which some gold (Au) nanoparticles were deposited. The Au nanoparticles harvest the Sunlight energy through a plasmonic effect. The energy absorbed by Au nanoparticles creates electrons and holes which excite the H_2O and CO_2 molecules adsorbed on CoO nanostructure surfaces to form excited hydrogen $(H_2)^*$ and excited carbon monoxide $(CO)^*$ on the CoO surface. The excited molecules combine to form CH_3OH on the CoO surface. The Au/CoO/Co nanostructured surfaces are useful for developing a low-cost method to convert solar energy to chemical energy in the form of methanol.

1. Introduction

Human society heavily relies on energy sources. Since the industrial revolution, industrial development and population growth have led to an enormous increase in the global demand for energy. Nowadays, various forms of energy resources have been discovered and utilized. For example, hydroelectric energy, wind energy and nuclear energy have been utilized [1–9]. These energies are converted into the electrical energy to fulfill the needs of modern society. But the application of electrical energy is usually limited by the problem of electrical energy storage lifetime and cost, for batteries usually have much lower specific energy (energy per unit mass) than fossil fuels. By comparison with internal combustion engines, electric motors are restricted from producing mechanical work with high efficiency [10–13]. In contrast, fossil fuels such as petroleum and natural gas are efficient energy forms. They are the primary sources of energy in the energy consumption all over the world. However fossil fuels are generally considered to be non-renewable resources because the nature of fossil fuels makes them unable to be replenished in a short period of time. In order to solve the energy shortage problem, scientists keep seeking to find the ways to produce energy with reduced production cost, simple manufacturing procedures and environmental friendly methods. There are many new technologies being developed. However, the high cost and the low efficiency of these new technologies makes them hard to be applied and industrialized. With the progress of science and technology, a newly developed technique provides an alternative way to solve the problem: artificial photosynthesis [14–21], which replicates the natural process of photosynthesis using chemical processes, converting solar energy into a form of chemical energy by photosynthesizing hydrocarbons or carbohydrates with water and carbon dioxide. The produced hydrocarbons are in the same form as the fuels made from the fossil fuel. As a result, the product can be easily utilized by current facilities.

In previous published papers, we have reported that a layer of flake-shaped, regular nanostructures can be formed on the surfaces cobalt microparticles of diameter of 50–100 μm by using the method of exposing them to

a femtosecond laser beam [22–31]. The cobalt microparticle powders with nanostructured surfaces can be used as a photocatalyst [31–33]. By using water and carbon dioxide as reactants, adjusting the experimental conditions such as temperature and pressure inside the reactor, hydrocarbons can be synthesized through this photocatalytic reaction with cobalt nanostructures. In this paper, we report that by changing the method of producing the photo-catalyst: we irradiated the cobalt powders by submerging them in the AuCl solution. After the laser treatment, not only a layer of blade-like sharp nanostructure was generated on the cobalt powder surface, but also a layer of gold nano-particles was formed and distributed on the surface of cobalt nanostructures. Via controlling the photocatalytic synthesis reaction conditions inside the reactor and taking the advantage of the enhancement of plasmonic nanofocusing [34–39] on the gold nanoparticles on the nanostructured Co micro-particle surface, the chemical bonds of H_2O and CO_2 can be broken or excited. Those excited molecules can eventually recombine to form methanol at low temperature. Furthermore, the specific surface area of the photocatalyst is dramatically enlarged after treating by this method, which results in a larger reaction surface for the chemical compound photo-dissociation and synthesis [40–42]. Through this procedure, the solar energy was converted to chemical energy, *i.e.* the solar energy is stored in the chemical bonds of methanol molecules.

Industrially, methanol can be synthesized on a large scale by fossil fuel based syngas [43, 44]. With many years of development, the technique became more and more mature, the costs kept decreasing. However, the technique requires high temperature and pressure which consume large amounts of energy and requires expensive manufacturing facilities. In the method used in this work, methanol can be produced under low pressure and temperature by only utilizing solar energy. By using this method, the carbon dioxide can be collected from air, thus keeps removing it from air and reducing the greenhouse effect.

2. Experimental method

Cobalt micro-powder (purity: 99.9%, size: 50–100 μm) surface laser treatment was carried out by using the Ti: sapphire femtosecond laser operating at a frequency of 1 kHz with pulse duration of 120 fs, a wavelength of 800 nm and an output power of 800 mW. Figure 1(a) shows that the Co powder was merged in a 3-ml 500-ppm gold chloride (AuCl) solution before the laser treatment. Figure 1(b) shows the experimental setup working with the femtosecond laser irradiation. The laser beam was irradiated on the Co micro particles merged in the AuCl solution that was filled in a fast spinning transparent glass vial driven by a motor. A very thin layer of cobalt microparticles was held on the wall of the glass vial while the glass vial is spinning. As a result, the surfaces of particles can be exposed to the laser beam uniformly. After laser irradiation, the Co micro-particles with nanostructures were dried in a venting vacuum chamber to prevent further possible oxidation of Co.

Figure 2 shows the photosynthesis setup. A 1.5-g catalyst made with femtosecond laser irradiation was loaded in a glass reactor (20 ml), and 350 mg of distilled water were filled into the reactor to cover the catalyst. Afterwards, the reactor was filled with 30 mg of CO_2 and sealed. A solar lamp for simulating natural sunlight (Honle, SOL 500) with a power density of 100 mW cm^{-2} was used to irradiate the nanostructured Co micro-particles in the sealed reactor at temperature of 50 °C for up to 10 h.

The surface structure of Co catalyst and its elemental composition were characterized and analyzed by a scanning electron microscopy (SEM) (JEOL, JSM 7401 F) equipped with energy-dispersive x-ray spectroscopy (EDXA Genesis XM2 imaging system with accelerating voltage of 15 kV). Before sample analysis, extraction was performed by first injecting 1-g of deuterated chloroform (chloroform-D, Sigma-Aldrich) into the reactor, then shaking until the product sufficiently solved in the solvent, finally separating the original water and solvent. Gas chromatography–mass spectrometry (GC-MS) analysis was carried out with a GC-MS instrument (Bruker, SCION SQ 436 equipped with a BR-5ms capillary column (30 m, 0.25 mm ID, 0.25 μm df)). To further confirm the result, a standard ^{13}C methanol and ^{13}C labeled sample were measured by a ^{13}C-Nuclear magnetic resonance (NMR) apparatus (Bruker & Spectrospin Avance DRX 500). Moreover, the water sample was analyzed by a total organic carbon (TOC) analyzer, (IONICS, 1444B carbon analyzer). By measuring the Total Carbon (TC) and Total Inorganic Carbon (TIC), the amount of harvested product can be calculated (TOC = TC- TIC). The result was further used to estimate the efficiency of this photocatalytic reaction.

3. Experimental result

Figures 3(a)–(c) shows surface morphology of the surface the Co microparticles after femtosecond laser irradiation. The scale bars are (a) 10 μm, (b) 1 μm, and (c) 100 nm, respectively. The original Co powder surface is rough, rugged but free of any nanostructures. After the laser treatment, nano-structures were generated and evenly distributed on the Co micro-particle surface. Figure 3(b) with higher magnification than figure (a) shows that the shape of those nanostructured Co is flake-like. The thickness of the nano-flakes is approximately

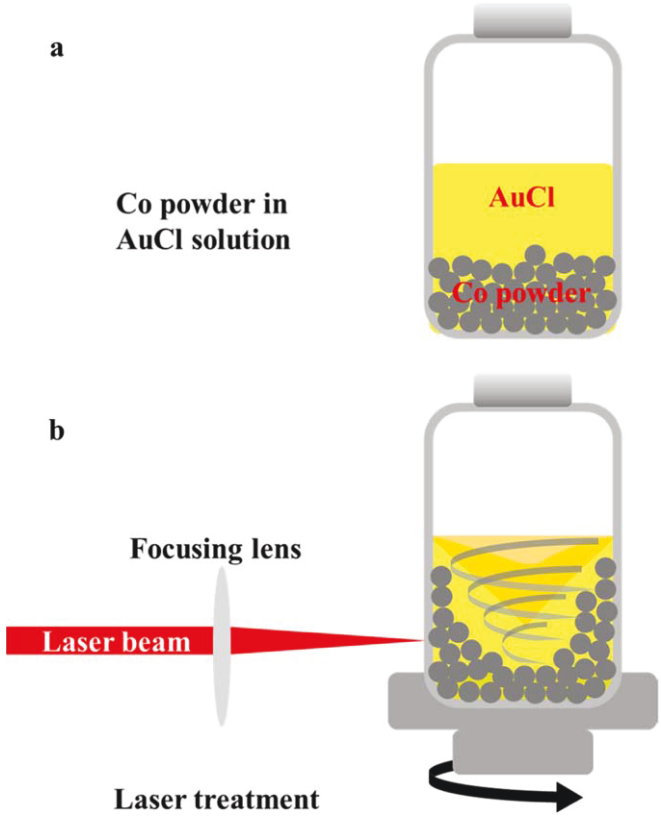

Figure 1. (a) Co micrparticle powders were merged in a 3-ml 500-ppm gold chloride (AuCl) solution before the laser treatment. (b) Experimental setup; a femtosecond laser beam was irradiated on the Co microparticles merged in the AuCl solution in the glass vial that was driven with a motor for a fast spinning motion.

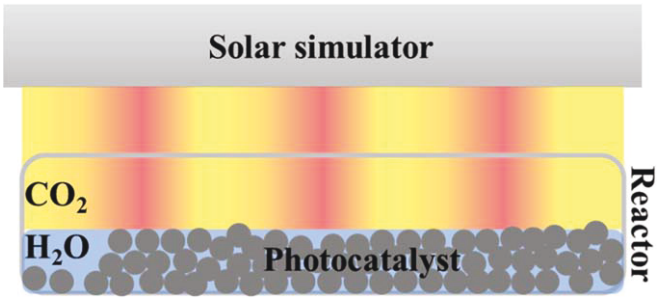

Figure 2. The nanostructured Co catalyst submerged in water was loaded in a glass vial filling with 1 atm CO_2 and the glass vial was sealed. Photocatalytic reactions were performed by exposing the glass vial to light from a solar simulator.

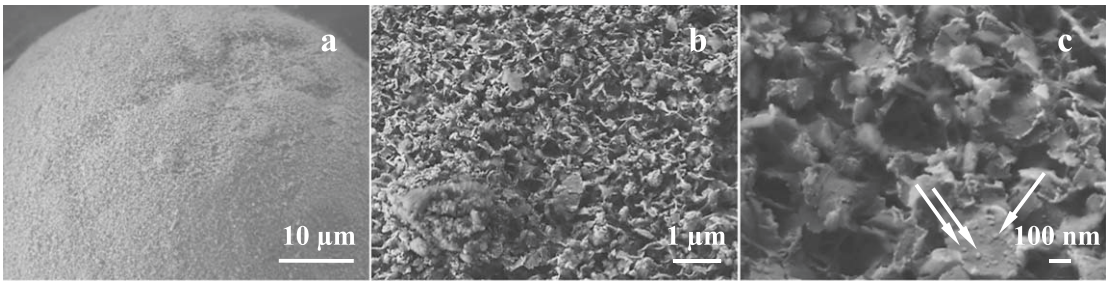

Figure 3. The morphology of Co surface after femtosecond laser irradiation. The scale bars are (a) 10 μm, (b) 1 μm, and (c) 100 nm, respectively. The arrows in figure 3(c) indicate the locations of Au nano-particles.

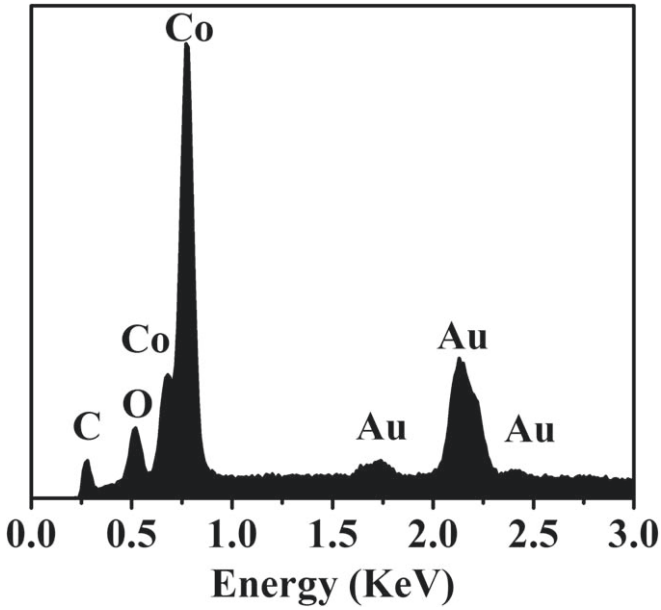

Figure 4. The Energy Dispersive x-ray Spectroscopy (EDS) analysis of the Au nanoparticle marked in figure 3(c). The result confirms that the small spots on the Co nanostructure's surface are Au nanoparitcles.

Table 1. The SEM/EDS analysis for the element composition at the position arrowed in figure 3(c).

Element	Wt%	At%
C	2.57	14.29
O	2.01	8.38
Co	56.48	64.10
Au	38.94	13.22
Total	100.00	100.00

5–10 nm. In addition, as indicated with arrows in figure 3(c), some smaller spots with the size in ten-nanometers, were observed deposit on the nano-flakes. As the CoO layer is too thin for the x-ray diffraction (XRD) measurement, the XRD spectra of the Co microparticles (supplementary data is available online at stacks.iop.org/MRX/7/035014/mmedia) show detection of only cobalt metal. The laser irradiation results in a significant lattice change in the cobalt surface. The cobalt particle surface before irradiation consisted of 33% hexagonal lattice structure and 67% cubic lattice structure. However, after the irradiation, it consisted of 77% hexagonal lattice structure and 23% cubic lattice structure. We need to study the chemical differences between cubic Co and hexagonal Co in the future.

Figure 4 shows an Energy Dispersive x-ray Spectroscopy (EDS) analysis of the nano-spots located on the Co nano-flakes marked in figure 3(c). Four elements were detected for both two areas. There are carbon, oxygen, cobalt and gold, respectively. The atomic ratio and weight ratio of the composition of bright part of Co nanostructure surface are listed in table 1.

The carbon element and oxygen element can also be found for untreated Co. The carbon element and oxygen element come from CO_2 adsorbed on the sample surface. Besides, although the sample was dried in a venting vacuum chamber, it can still be slightly oxidized after that, meaning that some cobalt oxide exists on the sample surface.

Moreover, for the gold signal, a thin film of Au was formed when dropping Co microparticles into the AuCl solution via single displacement reaction [45–47], since Co is much reactive than Au in reactivity series. Then during the femtosecond laser irradiation procedure, once the Au film was molten after the laser irradiation, the film tended to break up into Au nano-particles because a molten thin film on a solid surface was unstable [48–50]. That is also the reason why the places with that spot-like pattern own high Au concentration, whereas the places without that spot-like pattern own extremely low concentration of Au (less than 1% in Wt in the EDX measurement). Further confirmation of these Au particles with EDX mapping analysis is shown in the supplementary data.

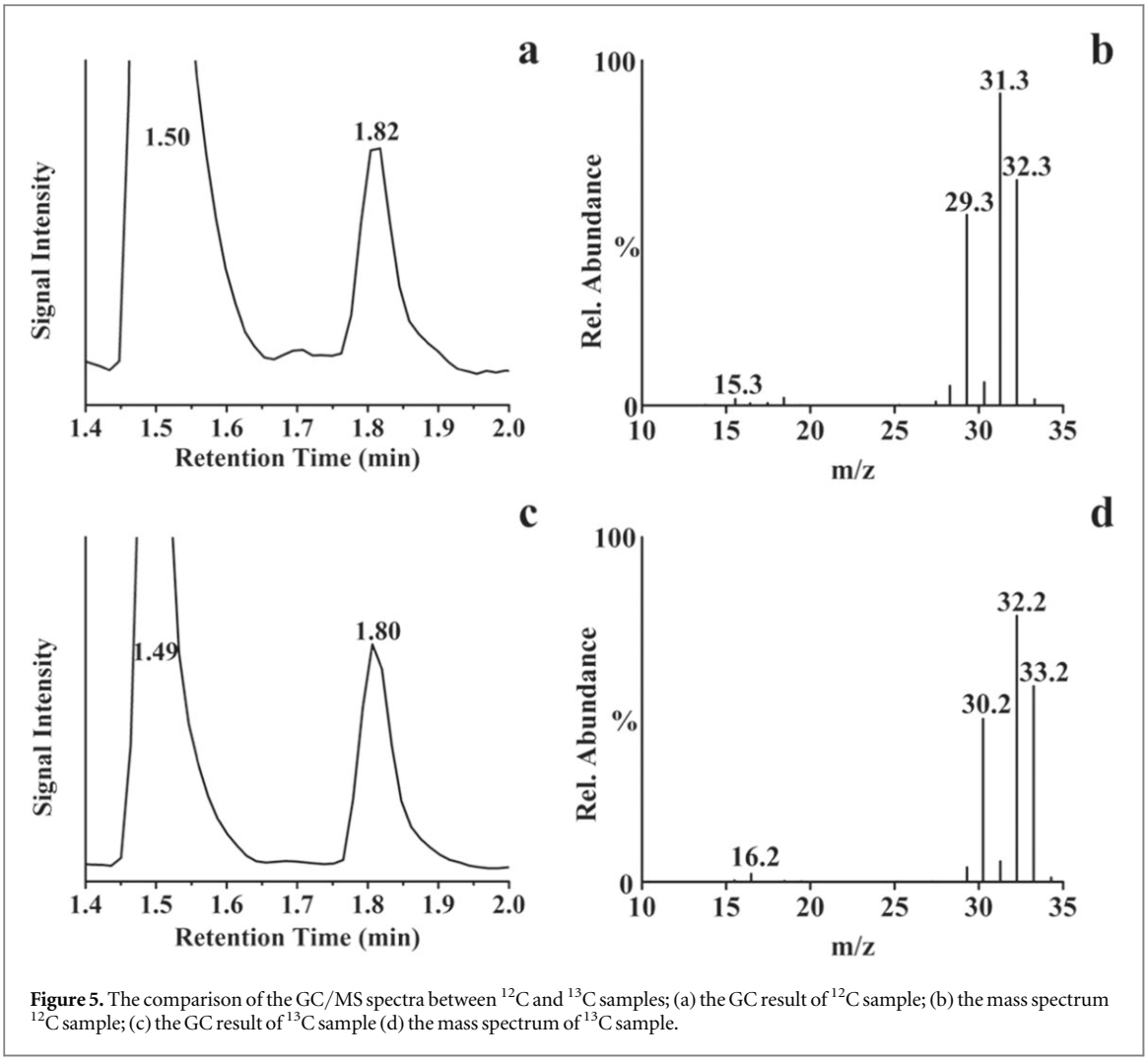

Figure 5. The comparison of the GC/MS spectra between ^{12}C and ^{13}C samples; (a) the GC result of ^{12}C sample; (b) the mass spectrum ^{12}C sample; (c) the GC result of ^{13}C sample (d) the mass spectrum of ^{13}C sample.

Figure 5 shows the GC-MS analysis of extraction solutions from the products using $^{12}CO_2$ and $^{13}CO_2$ gas as reactant. Figures 5(a) and (b) shows the GC spectrum of ^{12}C sample and the corresponding MS of the ^{12}C methanol. Figures 5(c) and (d) shows the GC spectrum of ^{13}C sample and corresponding MS of the ^{13}C methanol. As we can easily observe, in both figure 5(a) and c the water was detected, at retention time of 1.5 and 1.49 min respectively. This water originates from the extraction procedure, meaning small amount of water was solved in chloroform-D. The second peak at retention time of 1.82 min in figure 5(a) corresponds to the mass spectrum in figure 5(b). The molecular ion peak of 32.3 which corresponds to $[^{12}CH_3OH]^+$ ion in figure 5(b) is the characteristic mass spectrum of ^{12}C-methanol. The base peak of m/z 31.3 corresponds to $^{12}CH_3O^+$ fragment. Then under fragmentation, the peak of m/z 30.3 corresponding to $^{12}CH_2O^+$ fragment and 15.3 corresponding to $^{12}CH_3^+$ fragment can be observed in the mass spectra. For the second peak in figure 5(c) at retention time of 1.80 min corresponds to the mass spectrum shown in figure 5(d). By comparison the molecular ion peak of 33.2 which corresponding to $[^{13}CH_3OH]^+$ ion is the characteristic mass spectrum of ^{13}C methanol. The base peak of m/z 32.2 correspond to $^{13}CH_3O^+$ fragment. The peaks of m/z 31.2 and 16.2 as the derived fragments, corresponds to $^{13}CH_2O^+$ and $^{13}CH_3^+$ fragments, respectively. The comparison of ^{12}C methanol mass spectrum (figure 5(b)) with ^{13}C methanol mass spectrum (figure 5(d)) shows that the mass spectrum was shifted by one mass unit, this due to the fact that the ^{13}C methanol is one mass unit heavier than ^{12}C methanol.

Figure 6 shows the comparison of NMR analysis of commercially available standard ^{13}C methanol (Sigma) with our ^{13}C methanol sample. Figure 6(a) shows the standard ^{13}C methanol NMR spectrum. Figure 6(b) shows the ^{13}C methanol NMR spectrum of our sample. Besides, the solvent (chloroform-D) chemical shift at 77.0 ppm, the characteristic ^{13}C NMR shift at 50.0 ppm in both figures 6(a) and (b) clearly show that the existence of ^{13}C methanol in both standard ^{13}C methanol and in our sample. In addition, the $^{13}CO_2$ was also probed in our sample at 124.0 ppm, which is induced from the extraction procedure. Based on GS-MS analysis and NMR results, methanol can be identified and verified as the product of the nanostructured Co catalytic photosynthesis experiment.

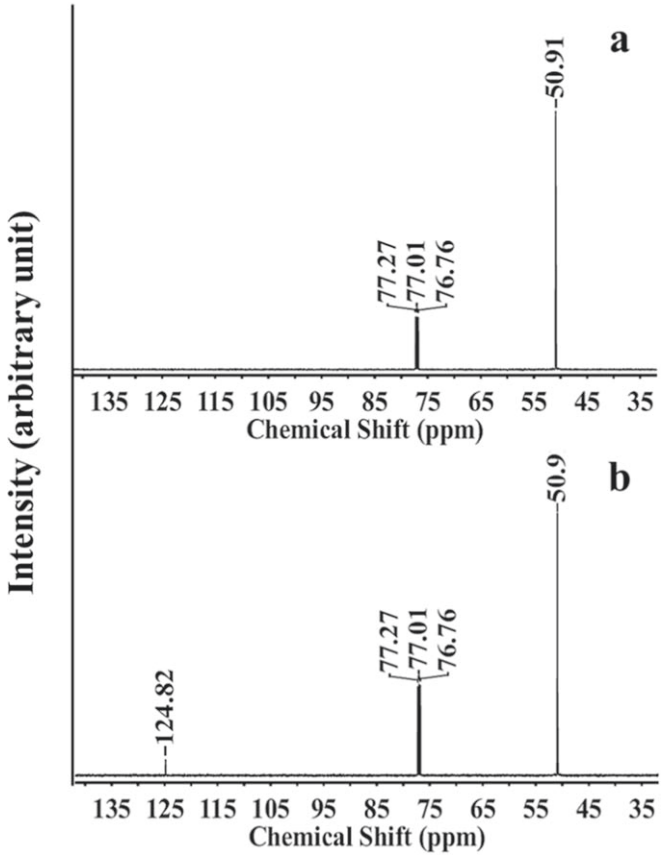

Figure 6. The comparison of NMR spectrum of standard ^{13}C methanol with that of our sample. (a) The NMR spectrum of standard ^{13}C methanol sample. (b) The NMR spectrum of our sample.

Moreover, in order to find a desirable experimental condition for forming the methanol product, a series of experiments was conducted using three types of photocatalyst and different reaction temperatures. Meanwhile the other experimental conditions and setups were kept the same as described in the experimental method section. The three types of photocatalyst are: Co microparticles, nanostructured Co microparticles and Au/Co nanostructured Co microparticles. The Co microparticle is used as the original commercial product. The nanostructured Co microparticle is synthesis by using the similar method as synthesis Au/Co nanostructured Co microparicles. The only difference is that the Co microparticles were merged in deionized water during the laser treatment. And the temperatures tested are separated to three parts. The first part is the temperature from room temperature to 50 °C, the second part is the temperature from 50 °C to 80 °C and the third part is the temperature from 80 °C to 120 °C. The temperature can be controlled and adjusted by changing the distance between the reactor and the solar simulator and using insulation material around the glass vial.

According to a series of experimental analysis, methanol can be detected for the sample using Au/Co nanostructured Co microparticle as photocatalyst. For the sample using only Co microparticle and nanostructured Co microparticle as photocatalyst, the GC/MS spectrum has not shown any methanol signal. As a result, the photocatalyst with Au nanoparticle combined with nanostructured Co microparticle is essential for catalyzing the formation of the methanol.

Moreover, from the analysis of a large amount of experimental results, we noticed that methanol can be hardly formed for the photosynthesis temperature lower than 50 °C. The necessary temperature for the formation of methanol is between 50 °C and 80 °C. In the reaction at a temperature between 80 °C and 120 °C, long-chain hydrocarbons were observed from the GC/MS measurement of the product, while methanol was not observed clearly. Therefore, the reaction temperature is an important controlling parameter to produce methanol.

TOC measurement quantized the methanol product in the photo-catalytic reaction. The solar-to-chemical energy efficiency has been obtained with the equation:

$$E = \frac{\text{Energy stored in the methanol}}{\text{Irradiation energy}} \quad (1)$$

Where the energy stored in the methanol was calculated from the heat of combustion of methanol (**22.7** J mg^{-1} [51]) multiplied by the mass of methanol products (**0.9** mg), and the irradiation energy was calculated as the solar intensity multiplied by the time and the irradiation area. In the glass pressure vessel, catalyst spread on the bottom had an irradiation area of about **4** cm^2. A solar-to-chemical energy efficiency was found to be about 0.3% for a five hour of solar irradiation.

4. Discussion

The GC analysis indicates trace amounts of CO in the photosynthesis process. Some oxygen was detected with an O_2 detector, although the precision was too low to quantify the detail, and further analysis using a gas chromatograph equipped with thermal conductivity detectors (GC-TCD) also revealed trace amounts of H_2. This is in agreement with the well-known water spitting process with photons and metal oxides. For example, CoO. CoO/Co can also be used for splitting water [31–33]. These observations support the existence of intermediate photodissociation processes where excited states or radicals are formed:

$$H_2O + \text{photons} \rightarrow (H_2)^* + \frac{1}{2}O_2 \quad (2)$$

$$CO_2 + \text{photons} \rightarrow (CO)^* + \frac{1}{2}O_2 \quad (3)$$

The denotation of $(\,)^*$ represents the molecule that is in a excited state (or in a form of radical) on the surface of CoO. As soon as $(H_2)^*$ and $(CO)^*$ are produced on the surface of CoO, methanol will form:

$$2(H_2)^* + (CO)^* \rightarrow CH_3OH \quad (4)$$

Only small amounts of $(H_2)^*$ and $(CO)^*$ may remain as detectable carbon monoxide and hydrogen gases since they are consumed in the hydrocarbon synthesis on the surface. The excited states or radicals $(H_2)^*$ and $(CO)^*$ that were confined around the CoO surface may not need high temperature and pressure to activate the reaction for methanol formation.

The optical absorption spectra measurements of both the CoO nano-flakes dispersed in water and the CoO nano-flakes on Co microparticles show band gaps at about 2.0 eV [33], which is smaller than that of a bulk crystal (about 2.4 eV) [52–55]. The spectra also show some absorption structures below the band gap [33]. The CoO nanoflakes have more defects than a bulk crystal, and the defects give rise to the different bandgap and the optical absorption below the bandgap [33]. For clarity, we do not consider the deformation of the electron band structure due to defects and simply show the simple energy diagram in figure 7 to discuss the processes occurring in the reaction. A CoO crystal is naturally p-type [56] because of Co vacancies; the concentration of this defect is much higher on the surface than deeper in the crystal. This effect leads to the hole energy levels of defects (green colored in figure 7) to be above the valence band but are still in the band gap. However, Co atoms at the Co/CoO interface diffuse into CoO and the self-interstitial Co atoms form high-density donors in CoO, which causes the CoO nanocrystals to be n-type [56–58]. This leads to O vacancies which form the electron energy levels of defects (orange colored in figure 7) below the conduction band of CoO but are still in the band gap.

Figure 7 shows the most likely illustration of the energy diagram for the photocatalytic processes. In both figures 7(a) and (b), the light energy was harvested by Au nanoparticles distributed on the surface of Co nano-flakes through the procedure of plasmonic nanofocusing, which provides the driving force to the following reaction. The lowest unoccupied molecular orbital (LUMO) state of carbon dioxide molecule adsorbed on CoO surface have been calculated [33]. It is found that the CO_2 molecule is chemisorbed on the CoO surface as the binding energy is 1.0 eV, the LUMO is found to be near the CoO conduction band (CB) bottom, and the the band gap of CoO is 2.38 eV. In figure 7(a), the highest occupied molecular orbital (HOMO) of CO_2 is far below the valence band (VB) top position of CoO; the LUMO of the CO_2 is shown to be very near to the conduction band (CB) bottom position of CoO [33, 59–61]. The electrons in the defect states (orange colored) of CoO are excited to the CB of CoO. The photo-excited electron quickly relaxes to the CB bottom where the LUMO is. Because the CO_2 and CoO are in the same system, the electron can efficiently transfer to the LUMO of CO_2 molecule that is adsorbed on the CoO, which results in $(CO_2)^-$, the electron attached state of CO_2.

In figure 7(b), the HOMO of the H_2O is below the valence band top of CoO. The LUMO of the H_2O is far above the CB top of CoO [19, 39, 59–62]. An electron is excited from the VB of CoO to the CoO defect states (green colored) that are above the VB top of CoO. The generated hole in the VB of CoO then transfers to the HOMO of H_2O molecules that are on the surface of CoO, which results in $(H_2O)^+$ [19, 39, 59–62]. Because the excited $(CO_2)^-$ and $(H_2O)^+$ molecules are not stable, they synthesize methanol or hydrocarbons on the CoO catalyst surfaces. The excited $(CO_2)^-$ and $(H_2O)^+$ molecules may also dissociate to form CO and H_2.

Figure 8 shows the most likely schematic diagram of artificial photosynthesis on the nanostructured Au/CoO surface. The blue peaks represent the CoO nano-flakes. The yellow spots represent the Au nanoparticles on

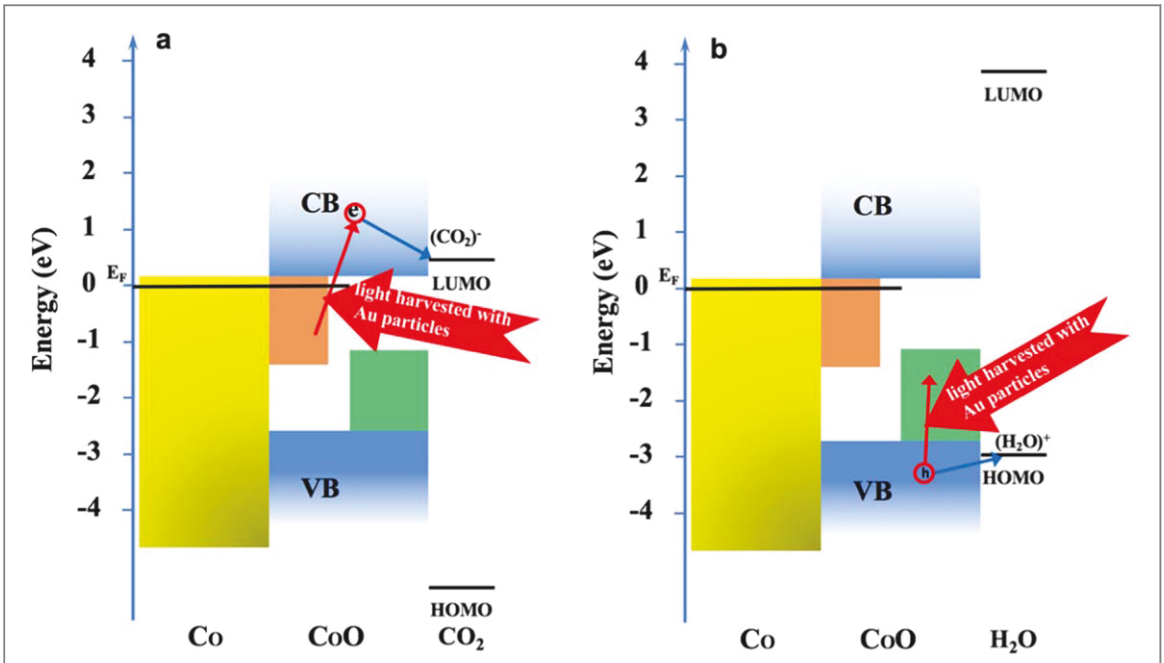

Figure 7. The energy diagram for the photocatalytic processes. a. An electron in the defect states of CoO are excited to the conduction band of CoO. The electron quickly relaxes to the CB bottom, then transfers to the LUMO of a CO_2 molecule that is adsorbed on the surface CoO, which results in the $(CO_2)^-$ the electron-attached state of CO_2. b. An electron was excited from the valence band of CoO to the defect states of CoO. The hole then transfers to the HOMO of H_2O that is on the surface of CoO, which results in the excited molecule $(H_2O)^+$.

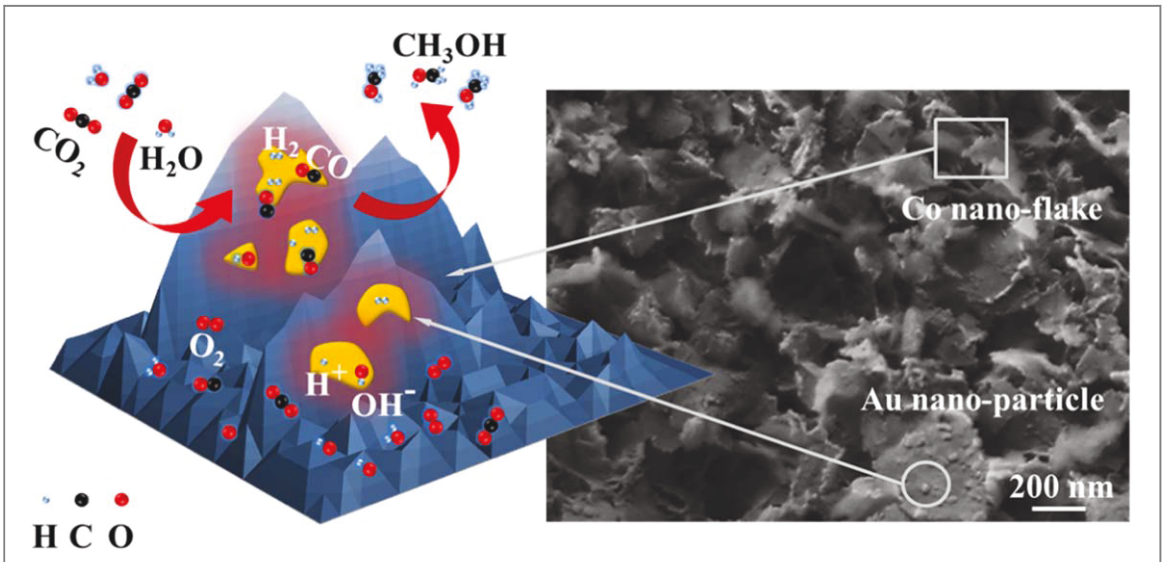

Figure 8. The most likely schematic diagram of chemical reactions on the Co surface. The incident solar light is firstly irradiated on and focused on the Au nanoparicles (marked by circle) formed on Co nano-flakes (shown by rectangle). The red area represents the local light intensity that is greatly increased by a surface plasmonic effect, while the blue represents that the area with relatively lower light intensity. The CO_2 and H_2O molecules attached to the surface are dissociated and the fragments react to form methanol.

the CoO nano-flakes' surface. The reactants such as H_2O and CO_2 are plotted as molecules surrounding Au nanoparticles and also distributed on the surface of the CoO nanostructure surface. Au nanoparticles play a very important role during the formation of methanol. The incident solar light is focused on Au nanoparticles via plasmonic nanofocusing [34–39], the local light intensity, represented by the red area, is greatly increased. The harvested light will dissociate the CO_2 and H_2O molecules as discussed above, the dissociated molecules will react to form methanol around the CoO surfaces.

The TOC test shows that the solar-to-chemical energy efficiency of our catalyst is about 0.3% in a five-hour irradiation. This is an average efficiency over five hours. Because the present reactor is a closed system, when the reactions reach an equilibrium state, the reaction hardly moves towards to the direction of producing more methanol. Several of the same samples and reactors for the photocatalytic reaction were irradiated for different

time durations to know methanol formation process. However, in this simple measurement, we could not clarify the process for when CO and H_2 were first produced and subsequently how they formed methanol. This needs further precise measurements to study the dynamics of how the methanol is synthesized from $(CO)^*$ and $(H2)^*$. After more than ten hours of irradiation, we cannot see any increase of the amount of methanol, *i.e.*, the production becomes saturated and leads to a low average efficiency. This is similar to the case of hydrocarbon production at a temperature between 80 °C and 120 °C. Considering this saturation effect, the average efficiency is estimated to be about 0.1%. For accurate efficiency, we will use an open system to directly measure the time dependence of the products without using the simple extraction method in this work. The efficiency of the photosynthesis may further increase by using a reactor that can perform continuous chemical reactions because an instantaneous efficiency may be very high. On the other hand, the photocatalyst can be made with CoO layer covering the Au nanostructured surfaces, which may collect more light with the enlarged surface of Au nanostructures and make the generated electrons and holes efficiently excite the CO_2 and H_2O molecules on the surface of CoO.

5. Summary

We discovered that femtosecond laser induced Au/Co nanostructures can convert CO_2 and H_2O to methanol through a photosynthesis process in a simple closed glass reactor that is transparent in visible wavelengths. The average efficiency of this process for solar-to-chemical energy conversion approached about 0.1% with a simple experimental setup and can be further improved by using a continuous reactor and optimizing the nanostructure morphologies. Further understanding of the mechanism in the present photocatalytic process will be helpful to achieve highly efficient solar energy storage on a large scale at low cost, which can be expected to have a profound impact on global energy requirements.

Acknowledgments

We thank Dr M Jayamanna for experimental assistance. And Dr D Ryan, Dr M Ruths, Dr L Li, Dr E Ada for helpful discussions. This research was supported by the National Science Foundation (CMMI-1161475 and CHE-1836540) and the United States Department of Energy.

ORCID iDs

Zhe Kan https://orcid.org/0000-0001-9454-7565
Mengyan Shen https://orcid.org/0000-0001-9884-4815

References

[1] Lenzen M 2008 *Energy Convers. Manage.* **49** 2178
[2] Hubbert M K 1956 Nuclear energy and the fossil fuel *Spring Meeting of the Southern District, Division of ProductionAmerican Petroleum Institute (Plaza Hotel, San Antonio, Texas , USA, March 7-8-9, 1956https://www.onepetro.org/conference-paper/API-56-007https://www.resilience.org/stories/2006-03-08/nuclear-energy-and-fossil-fuels/*
[3] Jacobson M Z 2009 *Energy & Environmental Science* **2** 148
[4] Herbert G M J, Iniyan S, Sreevalsan E and Rajapandian S 2007 *Renew. Sustain. Energy Rev.* **11** 1117
[5] Fung K T, Scheffler R L and Stolpe J 1981 *IEEE Trans Power Appar System* **100** 1176
[6] Ezio S and Claudio C 1998 *Journal of Wind Engineering and Industrial Aerodynamics* **74-76** 375
[7] Ackermann T and Söder L 2000 *Renewable and Sustainable Energy Reviews* **4** 315
[8] Kaldellis J K and Zafirakis D 2011 *Renewable Energy* **36** 1887
[9] Saidur R, Islam M R, Rahim N A and Solangi K H 2010 *Renew. Sustain. Energy Rev.* **14** 1744
[10] Dunn B, Kamath H and Tarascon J 2011 *Science* **334** 928
[11] Chen H, Cong T, Yang W, Tan C, Li Y and Ding Y 2009 *Prog. Nat. Sci.* **19** 291
[12] Thackeray M, Wolverton C and Isaacs E 2012 *Energy & Environmental Science* **5** 7854
[13] Hadjipaschalis I and A Poullikkas V E 2009 *Renew. Sustain. Energy Rev.* **13** 1513
[14] Gust D, Moore T and Moore A 2009 *Acc. Chem. Res.* **42** 1890
[15] Sun L, Hammarström L, Åkermark B and Styring S 2001 *Chem. Soc. Rev.* **30** 36
[16] Bolton J 1996 *Sol. Energy* **57** 37
[17] Alstrum-Acevedo H J, Brennaman M and T M 2005 *Inorg. Chem.* **44** 6802
[18] Imahori H, Mori Y and Matano Y 2003 *J. Photochem. Photobiol., C* **4** 51
[19] Tachibana Y, Vayssieres L and Durrant J 2012 *Nat. Photonics* **6** 511
[20] Chakraborty S, Wadas T, Hester H, Schmehl R and Eisenberg R 2005 *Inorg. Chem.* **44** 6865
[21] Benniston A and Harriman A 2008 *Mater. Today* **11** 26
[22] Her T, Finlay R, Wu C, Deliwala S and Mazur E 1998 *Appl. Phys. Lett.* **73** 1673
[23] Her T, Finlay R, Wu C and Mazur E 2000 *Appl. Phys.* A **70** 383

[24] Sheehy M, Winston L, Carey J, Friend C and Mazur E 2005 *Chem. Mater.* **17** 3582
[25] Shen M, Crouch C, Carey J and Mazur E 2004 *Appl. Phys. Lett.* **85** 5694
[26] Shen M, Carey J, Crouch C, Kandyla M, Stone H and Mazur E 2008 *Nano Lett.* **8** 2087
[27] Huo H and Shen M 2012 *J. Appl. Phys.* **112** 104314
[28] Kan Z, Zhang Q, Ren H and Shen M 2019 *Mater. Res. Express* **6** 085016
[29] Kan Z, Zhu Q, Ren H and Shen M 2019 *Materials* **12** 2043
[30] Wang C, Huo H, Johnson M, Shen M and Mazur E 2010 *Nanotechnology* **21** 075304
[31] Wang C, Shen M, Huo H, Ren H, Yan F and Johnson M 2009 *Int. J. Mod. Phys.* B **23** 5849 and Erratum, 28, 1492004 (2014)
[32] Wang C, Shen M, Huo H, Ren H and Johnson M 2011 *AIP Adv.* **1** 042124
[33] Wang C *et al* 2020 *Chem. Phys. Lett.* **739** 136985
[34] Stockman M 2004 *Phys. Rev. Lett.* **93** 137404
[35] Lindquist N, Nagpal P, Lesuffleur A, Norris D and Oh S 2010 *Nano Lett.* **10** 1369
[36] Berweger S, Atkin J, Olmon R and Raschke M 2012 *The Journal of Physical Chemistry Letters* **3** 945
[37] Linic S, Christopher P and Ingram D 2011 *Nat. Mater.* **10** 911
[38] Cushing S, Li J, Meng F, Senty T, Suri S, Zhi M, Li M, Bristow A and Wu N 2012 *JACS* **134** 15033
[39] Mukherjee S, Libisch F, Large N, Neumann O, Brown L, Cheng J, Lassiter J, Carter E, Nordlander P and Halas N 2012 *Nano Lett.* **13** 240
[40] Attard G, Bartlett P, Coleman N, Elliott J, Owen J and Wang J 1997 *Science* **278** 838
[41] Hirscher M and Panella B 2005 *J. Alloys Compd.* **404** 399
[42] Tang X, Liu Z, Zhang C, Yang Z and Wang Z 2009 *J. Power Sources* **193** 939
[43] Olah G, Goeppert A and Prakash G 2008 *The Journal of organic chemistry* **74** 487
[44] Lormand C 1925 *Ind. Eng. Chem.* **17** 430
[45] Chapman C 2001 *Eureka!: Success in Science* (Portsmouth, NH: Heinemann) Book 3
[46] Harwood R and Lodge I 2014 *Cambridge IGCSE Chemistry Coursebook.* (Cambridge: Cambridge University Press)
[47] Power G P and Ritchie I M 1975 *Modern Aspects of Electrochemistry* (*Metal displacement reactions*) 11 (New York: Plenum) pp. 199–250 ModernAspects of Electrochemistry
[48] Rayleigh L 1892 *The London, Edinburgh, and Dublin Philosophical Magazine and Journal of Science* **34** 145
[49] Plateau J A F 1873 *Statique expe×rimentale et the×orique des liquids soumis aux seules forces mole×culaires.* University Library Ghent
[50] Sharma A and Reiter G 1996 *J. Colloid Interface Sci.* **178** 383
[51] Haynes W M 2014 *CRC handbook of chemistry and physics.* (CRC press)
[52] Van Elp J, Wieland J L, Eskes H, Kuiper P, Sawatzky G A, De Groot F M F and Turner T S 1991 *Phys. Rev.* B **44** 6090–103
[53] Gillen R and Robertson J 2013 A hybrid density functional view of native vacancies in gallium nitride *Journal of Physics: Condensed Matter* **25** (40) 405501–8
[54] Hugel J and Kamal M 1996 *Solid State Comm.* **100** 457–61
[55] Powell R J and Spicer W E 1970 *Phys. Rev.* B **6** 2182–93
[56] Fisher B and Tannhauser D S 1966 *J. Chem. Phys.* **44** 1663–72
[57] Gvishi M and Tannhauser D S 1970 *Solid State Comm.* **8** 485–90
[58] Kim S H, Jeong S W, Hwang D K, Park S J and Seong T Y 2005 *Electrochem. Solid-State Lett.* **8** 198–200
[59] Pfennig B W 2015 *Principles of Inorganic Chemistry.* (New York: Wiley)
[60] Goddard III 2007 ed A William *et al Handbook of nanoscience, engineering, and technology.* (CRC press)
[61] Ching W and Rulis P 2012 *Electronic Structure Methods for Complex Materials: The Orthogonalized Linear Combination of Atomic Orbitals.* (Oxford: OUP)
[62] Grossman J C, Schwegler E, Draeger E W, Gygi F and Galli G 2004 *J. Chem. Phys.* **120** 300